science.sciencemag.org/cgi/content/full/science.abe1107/DC1

Supplementary Materials for

Preexisting and de novo humoral immunity to SARS-CoV-2 in humans

Kevin W. Ng, Nikhil Faulkner, Georgina H. Cornish, Annachiara Rosa, Ruth Harvey, Saira Hussain, Rachel Ulferts, Christopher Earl, Antoni G. Wrobel, Donald J. Benton, Chloe Roustan, William Bolland, Rachael Thompson, Ana Agua-Doce, Philip Hobson, Judith Heaney, Hannah Rickman, Stavroula Paraskevopoulou, Catherine F. Houlihan, Kirsty Thomson, Emilie Sanchez, Gee Yen Shin, Moira J. Spyer, Dhira Joshi, Nicola O'Reilly, Philip A. Walker, Svend Kjaer, Andrew Riddell, Catherine Moore, Bethany R. Jebson, Meredyth Wilkinson, Lucy R. Marshall, Elizabeth C. Rosser, Anna Radziszewska, Hannah Peckham, Coziana Ciurtin, Lucy R. Wedderburn, Rupert Beale, Charles Swanton, Sonia Gandhi, Brigitta Stockinger, John McCauley, Steve J. Gamblin, Laura E. McCoy*, Peter Cherepanov*, Eleni Nastouli*, George Kassiotis*

*Corresponding author. Email: george.kassiotis@crick.ac.uk (G.K.); e.nastouli@ucl.ac.uk (E.N.); peter.cherepanov@crick.ac.uk (P.C.); l.mccoy@ucl.ac.uk (L.E.M.)

Published 6 November 2020 on *Science* First Release
DOI: 10.1126/science.abe1107

This PDF file includes:

Other Supplementary Material for this manuscript includes the following:
(available at science.sciencemag.org/cgi/content/full/science.abe1107/DC1)

MDAR Reproducibility Checklist (PDF)

Materials and Methods

Patients and clinical samples

Serum or plasma samples were obtained from University College London Hospitals (UCLH) COVID-19 patients testing positive for SARS-CoV-2 infection by RT-qPCR and sampled between March 2020 and April 2020. An initial cohort of 35 patients (31 annotated) and an extended cohort of 135 patients were tested between 2 and 43 days after the onset of COVID-19 symptoms (Table S1). A total of 305 samples from 302 SARS-CoV-2-uninfected adults and 48 samples from SARS-CoV-2-uninfected children and adolescents were also used (described in Table S1). Samples from adults were obtained from UCLH (ref 284088) and Public Health Wales, University Hospital of Wales, and samples from children, adolescents, and young adults were obtained from the Centre for Adolescent Rheumatology Versus Arthritis at University College London (UCL), UCLH, and Great Ormond Street Hospitals (GOSH), and Great Ormond Street Institute for Child Health (ICH) with ethical approval (refs 11/LO/0330 and 95RU04). All patient sera and sera remaining after antenatal screening of healthy pregnant women were from residual samples prior to discarding, in accordance with Royal College Pathologists guidelines and the UCLH Clinical Governance for assay development and GOSH and ICH regulations. All pre-pandemic samples had undergone at least one cycle of thaw and freeze, and had been stored at either −20°C or −80°C freezers at local hospitals prior to transfer (on dry ice) to the Francis Crick Institute. All serum or plasma samples were heat-treated at 56°C for 30 min prior to testing.

Viral infection RT-qPCR diagnosis

SARS-CoV-2 nucleic acids were detected in nasopharyngeal swabs by a diagnostic RT-qPCR assay using custom primers and probes (*18*), with sensitivity comparable to the Panther Fusion (Hologic) automated platform, and a limit of detection of approximately 1×10^{-2} tissue culture infective dose $(TCID)_{50}$/ml. HCoV nucleic acids were detected by RT-qPCR, as part of a diagnostic panel for respiratory viruses. Assays were run by Health Services Laboratories (HSL), London, UK and Public Health Wales Microbiology, UK.

Cell lines and virus

HEK293T and K-562 cells were obtained from the Cell Services facility at The Francis Crick Institute, verified as mycoplasma-free and validated by DNA fingerprinting. Vero-E6 cells were from the National Institute for Biological Standards and Control, UK. HEK293T cells overexpressing ACE2 were generated by transfection, using GeneJuice (EMD Millipore), with a plasmid containing the complete human ACE2 transcript variant 1 cDNA sequence (NM_001371415.1) cloned into the mammalian expression vector pcDNA3.1-C' FLAG by Genscript. HEK293T cells expressing HERV-K113 envelope glycoprotein were generated by retroviral transduction with the vector encoding the putative ancestral protein sequence of HERV-K113 envelope glycoprotein (*19*) and GFP separated by an internal ribosome entry site (IRES). Transduced cells were sorted based on GFP expression to >98% purity on a FACSAria Fusion cell sorter (Beckton Dickinson) and maintained as a cell line. Cells were grown in Iscove's Modified Dulbecco's Medium (Sigma Aldrich) supplemented with 5% fetal bovine serum (Thermo Fisher Scientific), L-glutamine (2 mM, Thermo Fisher Scientific), penicillin (100 U/ml, Thermo Fisher

Scientific), and streptomycin (0.1 mg/ml, Thermo Fisher Scientific). The SARS-CoV-2 isolate hCoV-19/England/02/2020 was obtained from the Respiratory Virus Unit, Public Health England, UK, (GISAID EpiCov^{TM} accession EPI_ISL_407073) and propagated in Vero E6 cells.

Flow cytometry

HEK293T cells were transfected with an expression vector (pcDNA3) carrying a codon-optimized gene encoding the wild-type SARS-CoV-2 S (UniProt ID: P0DTC2) (kindly provided by Massimo Pizzato, University of Trento, Italy), using GeneJuice (EMD Millipore). Similarly, HEK293T cells were transfected with expression vectors (pCMV3) expressing HCoV-229E S (UniProt ID: APT69883.1), HCoV-NL63 S (UniProt ID: APF29071.1), HCoV-OC43 S (UniProt ID: AVR40344.1) or HCoV-HKU1 S (UniProt ID: Q0ZME7.1) (all from SinoBiological). Two days after transfection, cells were trypsinized and transferred into V-bottom 96-well plates (20,000 cells/well). Cells were incubated with sera (diluted 1:50 in PBS) for 30 min, washed with FACS buffer (PBS, 5% BSA, 0.05% sodium azide), and stained with BV421 anti-IgG (clone HP6017, Biolegend), APC anti-IgM (clone MHM-88, Biolegend) and PE anti-IgA (clone IS11-8E10, Miltenyi Biotech) for 30 min (all antibodies diluted 1:200 in FACS buffer). Cells were washed with FACS buffer and fixed for 20 min in CellFIX buffer (BD Bioscience). Samples were run on a Ze5 analyzer (Bio-Rad) running Bio-Rad Everest software v2.4 or an LSR Fortessa with a high-throughput sampler (BD Biosciences) running BD FACSDiva software v8.0, and analyzed using FlowJo v10 (Tree Star Inc.) analysis software. Transfection efficiencies were determined by staining with a fixed concentration of the S1-reactive CR3022 antibody (human IgG1) (100 ng/ml) (Absolute Antibodies) and control COVID-19 convalescent sera (1:50 dilution), followed by BV421 anti-human IgG antibody. In some experiments, SARS-CoV-2 S expression in transfected cells was additionally determined by staining with the S2-reactive D001 antibody (40590-D001, SinoBiological), which is a chimeric antibody using murine variable domains fused to human IgG1 constant region. The CR3022 antibody binds an epitope in S1 only in the 'open' conformation (*20, 21*). Staining with convalescent sera, detecting epitopes over the entire S ectodomain, was consistently higher than staining with CR3022 and was taken as the maximum transfection efficiency. This varied between 68% and 95% between experiments. Specifically for the experiments involving blocking with recombinant soluble S1 and S2 proteins, a lower transfection efficiency of approximately 50% was used to facilitate gating based on sufficient untransfected cells in the population. For these experiments, 10 µg/ml of soluble S1 (made in-house, see below Recombinant protein production) or soluble S2 ($S_{686-1273}$, CV2006, LifeSensors) were added to the cells during incubation with sera. As an additional control for staining specificity, HEK293T cells transfected to express SARS-CoV-2 S were mixed at equal ratios with HEK293T cells stably expressing the a HERV-K envelope glycoprotein and GFP. The cells were distinguished on flow cytometry based on GFP expression. SARS-CoV-2 S-reactive antibody titers varied by several orders of magnitude among COVID-19 convalescent sera, with some reliably detected only at the highest serum concentration (1:50 dilution). Consequently, this dilution was used for subsequent sensitive measurements. Although the intensity of IgM and IgG staining decreased proportionally with serum dilutions, the intensity of IgA staining peaked at intermediate serum dilutions, likely owing to competition with IgG antibodies at higher serum concentrations. Thus, the

intensity of staining with each of the three main Ig classes may reflect their relative ratios, as well as their absolute titers. By contrast, the percentage of cells stained with each Ig class was less sensitive to serum dilutions and was chosen as a correlate for seropositivity.

Recombinant protein production

The SARS-CoV-2 RBD and S1 constructs, spanning SARS-CoV-2 S (UniProt ID: P0DTC2) residues 319-541 (RVQPT…KCVNF) and 1-530 (MFVFL…GPKKS), respectively, were produced with C-terminal twin Strep tags. To this end, the corresponding codon-optimised DNA fragments were cloned into mammalian expression vector pQ-3C-2xStrep (*22*). A signal peptide from immunoglobulin kappa gene product (METDTLLLWVLLLWVPGSTGD) was used to direct secretion of the RBD construct. Stabilised ectodomain of the SARS-CoV-2 S glycoprotein (residues 1-1208) with inactivated furin cleavage site (RRAR, residues 682-685 mutated to GSAS) and a double proline substitution (K986P/V987P) (*23, 24*) was produced with a C-terminal T4 fibritin trimerization domain and a hexahistidine (His_6) tag from the pcDNA3 vector. Expi293F cells growing at 37°C in 5% CO_2 atmosphere in shake flasks in FreeStyle 293 medium were transfected with the corresponding plasmids using ExpiFectamine reagent (Thermo Fisher Scientific). Conditioned medium containing secreted proteins was harvested twice, 3-4 and 6-8 days post-transfection. Twin Strep- and His_6- tagged proteins were captured on Streptactin XT (IBA LifeSciences) or Talon (Takara) affinity resin, respectively, and purified to homogeneity by size exclusion chromatography through Superdex 200 (GE Healthcare) in 150 mM NaCl, 1 mM EDTA, and 20 mM Tris-HCl, pH 8.0. Full-length SARS CoV2 N gene product was produced with an N-terminal His_6 tag from pOPTH-1124 plasmid (kindly provided by Jakub Luptak and Leo James, Laboratory for Molecular Biology, Cambridge, UK). *Escherichia coli* C43(DE3) cells (Lucigen) transformed with pOPTH-1124 were grown in terrific broth medium, and expression was induced by addition of 1 mM Isopropyl β-D-1-thiogalactopyranoside at 37°C. Bacteria, harvested 4 hours post-induction, were disrupted by sonication in core buffer (1 M NaCl, 10 mM imidazole, 20 mM HEPES-NaOH, pH 8.0) supplemented with BaseMuncher nuclease (Expedion; 1 ml per 40 ml of cell suspension) and Complete EDTA-free protease inhibitor mix (Roche). The extract was precleared by centrifugation at 45,000×*g* for 45 min, and His_6-tagged protein was captured on NiNTA agarose (Qiagen). Following extensive washes with core buffer supplemented with 20 mM imidazole, the protein was eluted with 500 mM imidazole. SARS CoV-2 N, was further purified by cation exchange and heparin affinity chromatography prior polishing by gel filtration through a Superdex 200 16/40 column (GE Healthcare), which was operated in 300 mM NaCl, 20 mM HEPES-NaOH, pH 8.0. Purified SARS CoV2 antigens, concentrated to 1-5 mg/ml by ultrafiltration using appropriate VivaSpin devices (Sartorius), were snap-frozen in liquid nitrogen in small aliquots and stored at −80°C.

ELISA

Ninety-six-well MaxiSorp plates (Thermo Fisher Scientific) were coated overnight at 4°C with purified protein in PBS (3 µg/ml per well in 50 µl) and blocked for 1 hour in blocking buffer (PBS, 5% milk, 0.05% Tween 20, and 0.01% sodium azide). Sera were diluted in blocking buffer (1:50). Fifty microliters of serum was then added to the plate and

incubated for 1 hour at room temperature. After washing four times with PBS-T (PBS, 0.05% Tween 20), plates were incubated with alkaline phosphatase-conjugated goat anti-human IgG (1:1000, Jackson ImmunoResearch) for 1 hour. Plates were developed by adding 50 µl of alkaline phosphatase substrate (Sigma Aldrich) for 15-30 min after six washes with PBS-T. Optical densities were measured at 405 nm on a microplate reader (Tecan). CR3022 (Absolute Antibodies) was used as a positive control for ELISAs coated with S, S1, and RBD. For ELISAs with synthetic peptides, 96-well Nunc Immobilizer Amino Plates (Thermo Fisher Scientific) were used for coating overnight at 4°C with peptides (10 µg/ml per well in 50 µl)

Lentiviral particle production and neutralization

Lentiviral particles pseudotyped with either SARS-CoV-2 S or Vesicular Stomatitis Virus glycoprotein (VSVg) were produced by co-transfection of HEK293T cells with plasmids encoding either of these glycoproteins together with a plasmid encoding the SIVmac Gag-Pol polyprotein and a plasmid expressing an HIV-2 backbone with a GFP encoding gene, using GeneJuice (EMD Millipore). Virus-containing supernatants were collected 48 hours post-transfection and stored at −80°C until further use. For neutralization assays, lentiviral pseudotypes were incubated with serial dilutions of patient sera at 37°C for 30 min and were subsequently added to HEK293T cells seeded in 96-well plates (3,000 cells/well). Polybrene (4 µg/ml, Sigma Aldrich) was also added to the cells and plates were spun at 315×*g* for 45 min. The percentage of transduced (GFP^+) cells was assessed by flow cytometry 72 hours later. The inverse serum dilution leading to 50% reduction of GFP^+ cells was taken as the neutralizing titer.

SARS-CoV-2 plaque reduction neutralization test

Confluent monolayers of Vero E6 cells were incubated with 10-20 plaque-forming units (PFU) of SARS-CoV-2 strain hCoV-19/England/2/2020 and twofold serial dilutions of human sera (previously heat-treated at 56°C for 30 min) starting at 1:40 dilution for 3 hours at 37°C, 5% CO_2, in triplicate per condition. The inoculum was then removed and cells were overlaid with virus growth medium containing 1.2% Avicel (FMC BioPolymer). Cells were incubated at 37°C, 5% CO_2. At 24 hours post-infection, cells were fixed in 4% paraformaldehyde and permeabilized with 0.2% Triton X-100/PBS. Virus plaques were visualized by immunostaining, as described previously for the neutralization of influenza viruses (*25*), except using a rabbit polyclonal anti-NSP8 antibody (antibodies-online, catalogue number ABIN233792, used at 1:1,000 dilution) and anti-rabbit-HRP conjugated antibody (Bio-Rad, catalogue number 1706515, used at 1:1,000 dilution) and detected by action of HRP on a tetra methyl benzidine (TMB) based substrate. Virus plaques were quantified and IC_{50} for sera was calculated using LabView software as described previously (*25*).

Antibody-dependent enhancement assay

For ADE assays, SARS-CoV-2 S lentiviral pseudotypes were incubated with patient sera diluted at 1:50 at 37°C for 30 min and were subsequently added to K-562 cells seeded in 96-well plates (3,000 cells/well) with polybrene (4 µg/ml, Sigma Aldrich) and anti-human CD32A (IV.3, StemCell) as indicated. The percentage of transduced cells (GFP^+)

was assessed by flow cytometry 72 hours later. VSVg and ecotropic murine leukemia virus (MLV) envelope glycoprotein (eMLV gp70) pseudotypes were used as controls. ADE was mediated by serially diluted anti-VSVg antibodies (clone 8G5F11, Kerafast) and anti-MLV envelope glycoprotein antibodies (83A25, purified in-house) (*26*), respectively.

Peptide arrays

Peptide arrays spanning the last 743 amino acids of SARS-CoV-2 S were constructed as 12-mers overlapping by 10 amino acid residues. Peptide arrays were synthesized on an Intavis ResPepSL Automated Peptide Synthesizer (Intavis Bioanalytical Instruments, Germany) on a cellulose membrane by cycles of N(a)-Fmoc amino acids coupling via activation of carboxylic acid groups with diisopropylcarbodiimide (DIC) in the presence of Ethyl cyano(hydroxyimino)acetate (Oxyma pure) followed by removal of the temporary α-amino protecting group by piperidine treatment. Subsequent to chain assembly, side chain protection groups were removed by treatment of membranes with a deprotection cocktail (95% trifluoroacetic acid, 3% triisopropylsilane, and 2% water in a 20-ml volume for 4 hours at room temperature) then washing (four times DCM, four times EtOH, twice H_2O, and once EtOH) prior to being air dried. Membranes were blocked for 1 hour in blocking buffer (PBS, 5% BSA, 0.05% Tween 20, 0.05% sodium azide), then stained with pooled sera (1:100 dilution in blocking buffer) for 2 hours at room temperature. Membranes were washed three times in PBS-T, then stained with IRDye 800CW Goat anti-Human IgG (Licor; 1:15,000 in blocking buffer) for 1 hour at room temperature in the dark. Membranes were washed three times in PBS-T and once in PBS before imaging on an Odyssey CLx Infrared scanner (Licor). Scanned images were analyzed in Image Studio v5.2 (Licor).

Individual peptide synthesis

Individual peptides were synthesized on an Intavis ResPepSLi Automated Peptide Synthesizer (Intavis Bioanalytical Instruments, Germany) on Rink amide resin (0.26 mmole/g, 0.1 mmol) using N(a)-Fmoc amino acids and HATU as the coupling reagent. Following amino acid chain assembly, peptides were cleaved from the resin by addition to cleavage cocktail (92.5% TFA, 2.5% H_2O, 2.5% EDT, and 2.5% TIS in a 10-ml volume) for 2 hours. Following resin removal, peptide precipitation and extensive washing with ether, the peptides were analysed by LC–MS on an Agilent 1100 LC-MSD.

Data analysis

Data were analyzed and plotted in GraphPad Prism v8 (GraphPad Software) or SigmaPlot v14.0 (Systat Software). Sequence alignments were performed with Vector NTI v11.5 (Thermo Fisher Scientific).

Supplementary Text

Entry of SARS-CoV-2 S-pseudotyped lentiviral particles into HEK293T cells

SARS-CoV-2 binding to one identified cellular receptor, angiotensin-converting enzyme 2 (ACE2) (*27-30*), is mediated by the RBD. Entry of SARS-CoV-2 has also been suggested to be facilitated by the alternative receptor CD147, also known as basigin (BSG) (*31*), neuropilin 1 (*32, 33*), and possibly also by receptor-independent mechanisms, as has been described for other CoVs (*34, 35*). HEK293T cells lack ACE2 expression, but are nevertheless permissive to entry of lentiviral particles pseudotyped with SARS-CoV-2 S (**fig. S14**). Moreover, transduction efficiency of HEK293T cells by SARS-CoV-2 S pseudotypes was not further increased by ACE2 overexpression (**fig. S14**), highlighting ACE2-independent entry. In contrast, HEK293T cells expressed high levels of *BSG* and *NRP1*, encoding CD147 and neuropilin 1, respectively (**fig. S14**).

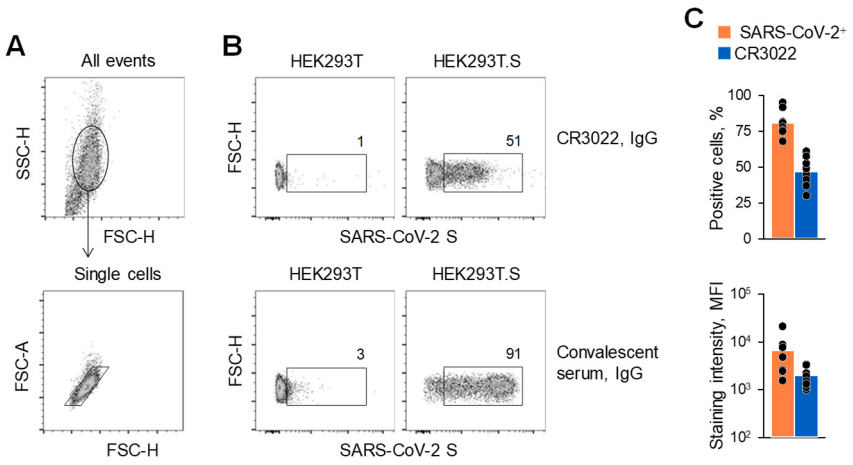

Fig. S1. Detection of cell membrane-bound SARS-CoV-2 S by flow cytometry.

HEK293T cells were transfected with an expression plasmid encoding the wild-type SARS-CoV-2 S and two days later were used for flow cytometry analysis. (**A**) Gating of HEK293T cells and of single cells in cell suspensions. (**B**) Representative staining of untransfected HEK293T cells or SARS-CoV-2 S-transfected HEK293T cells (HEK293T.S) with either the CR3022 monoclonal antibody or serum from COVID-19 patients as the primary antibody, followed by an anti-human IgG secondary antibody. (**C**) Percentage of positive cells (top) and mean fluorescence intensity (MFI) (bottom) of staining with either the CR3022 antibody or COVID-19 patient serum in 8 independent experiments. The differences in the percentage of positive cells and MFI were statistically significant with P=0.000008, paired t test and P=0.008, Wilcoxon Signed-Rank Test, respectively.

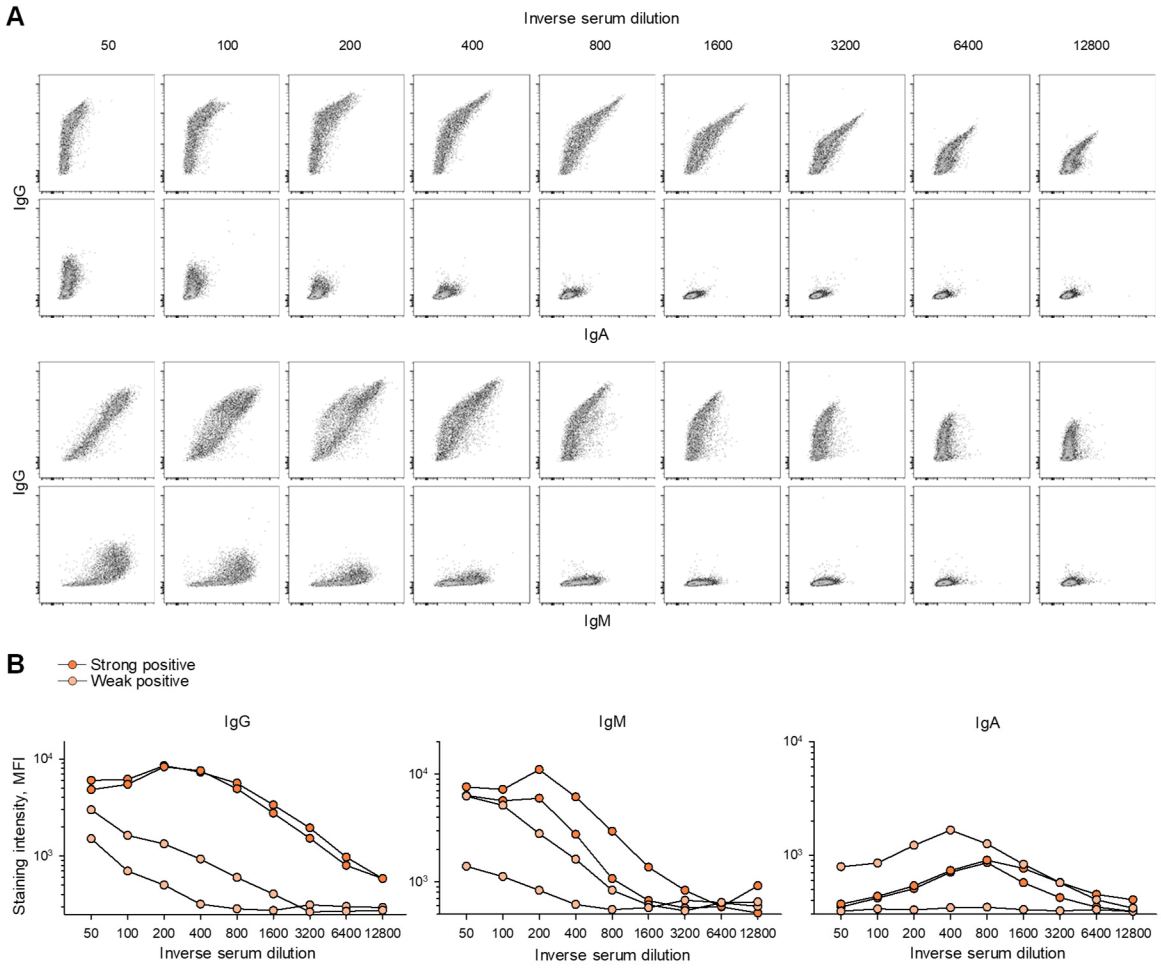

Fig. S2. Detection of SARS-CoV-2 S-binding IgG, IgM and IgA antibodies by flow cytometry.

(**A**) Flow cytometry profiles of SARS-CoV-2 S-transfected HEK293T cells stained with the indicated serial dilutions of COVID-19 patient sera selected to represent the high (top row in each panel) and low (bottom row in each panel) ends of detection at 1:50 dilution. (**B**) MFI of IgG, IgM and IgA staining, according to the indicated serial dilution of two samples from each end of the detection range. Each line represents an individual COVID-19 patient serum sample.

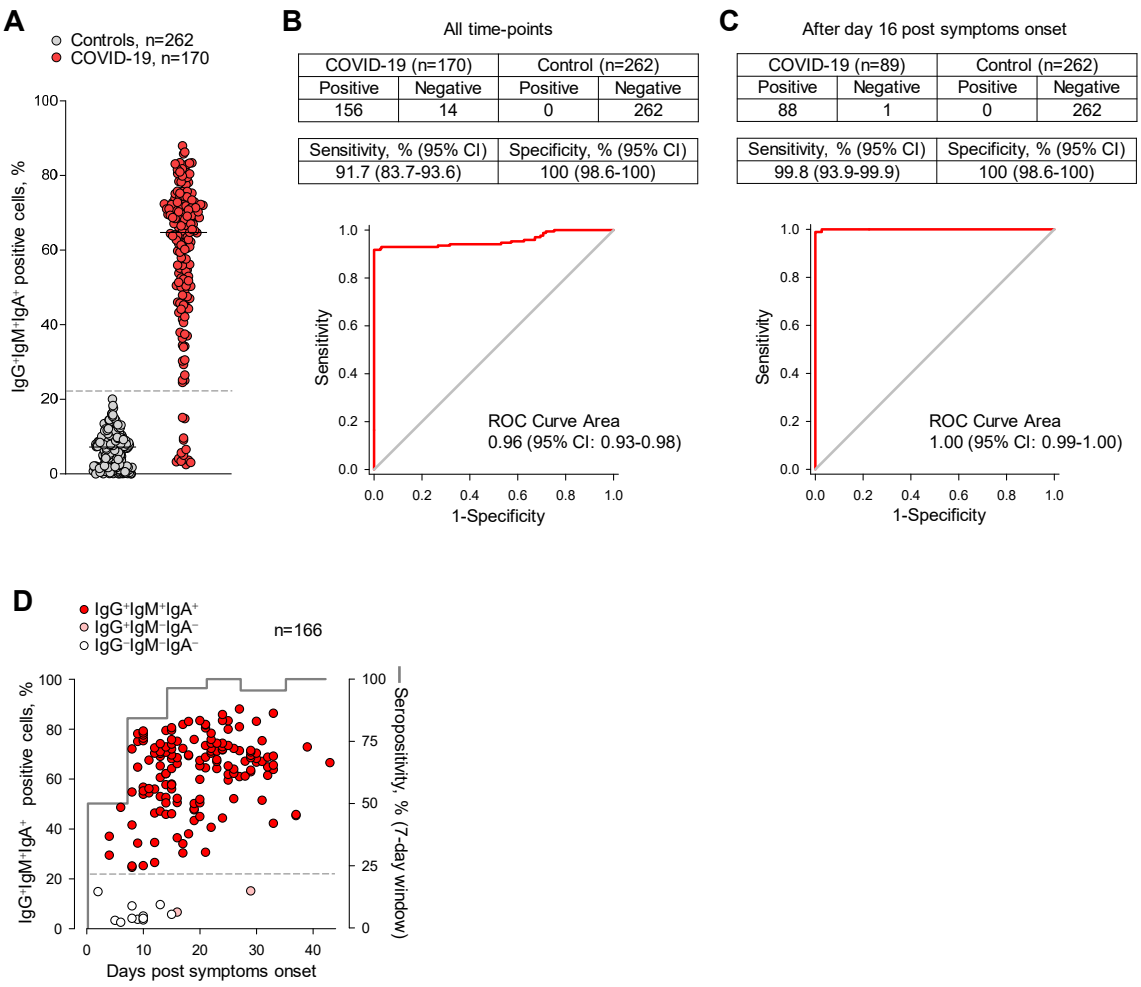

Fig. S3. Performance of the flow cytometry-based assay for SARS-CoV-2-reactive antibody detection.

(**A**) Frequency of SARS-CoV-2 S-transfected HEK293T cells that stained positive with all three antibody classes ($IgG^+IgM^+IgA^+$) with sera from 170 confirmed COVID-19 cases at University College London Hospitals (UCLH) and 262 controls. The dashed line represents the calculated cut-off for positivity. (**B** and **C**) Sensitivity and specificity for the assay calculated for all the sample collected at any time-point post symptom onset (B) or only for samples collected 16 days after the onset of COVID-19 symptoms (C). The receiver operating characteristics (ROC) curve areas and 95% confidence intervals (CI) are also shown for each group. (**D**) Kinetics of seroconversion in COVID-19 patients determined by the flow cytometry-based assay. Percentages of $IgG^+IgM^+IgA^+$ positive cells are plotted over time of sample collection since symptom onset. Seropositivity was calculated for each consecutive week since symptom onset. Only COVID-19 patients with known date of symptom onset are included.

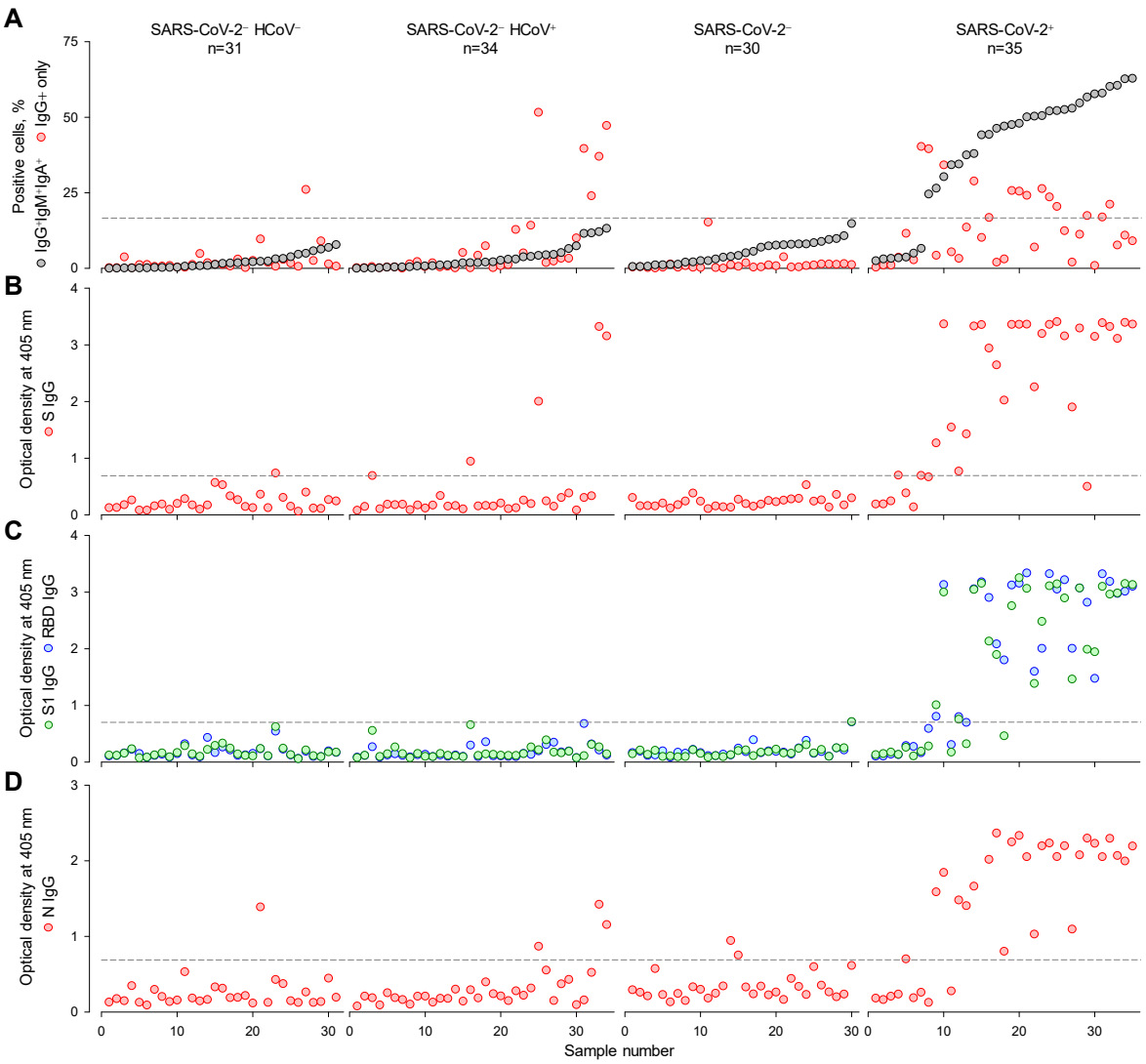

Fig. S4. Comparison of antibody detection methods using a panel of patient samples.

Serum samples from the following groups were compared in all panels: SARS-CoV-2-uninfected without recent HCoV infection (SARS-CoV-2$^-$ HCoV$^-$); SARS-CoV-2-uninfected with recent HCoV infection (SARS-CoV-2$^-$ HCoV$^+$); SARS-CoV-2-uninfected with unknown history of recent HCoV infection (SARS-CoV-2$^-$); SARS-CoV-2-infected (SARS-CoV-2$^+$). (**A**) Frequency of cells that stained with all three antibody classes (IgG$^+$IgM$^+$IgA$^+$) or only with IgG (IgG$^+$) in each of these samples, ranked by their IgG$^+$IgM$^+$IgA$^+$ frequency. (**B** to **D**) Optical densities from ELISAs coated with S (B), S1 or RBD (C) or N (D) of the same samples. Dashed lines in A to D denote the assay sensitivity cut-offs.

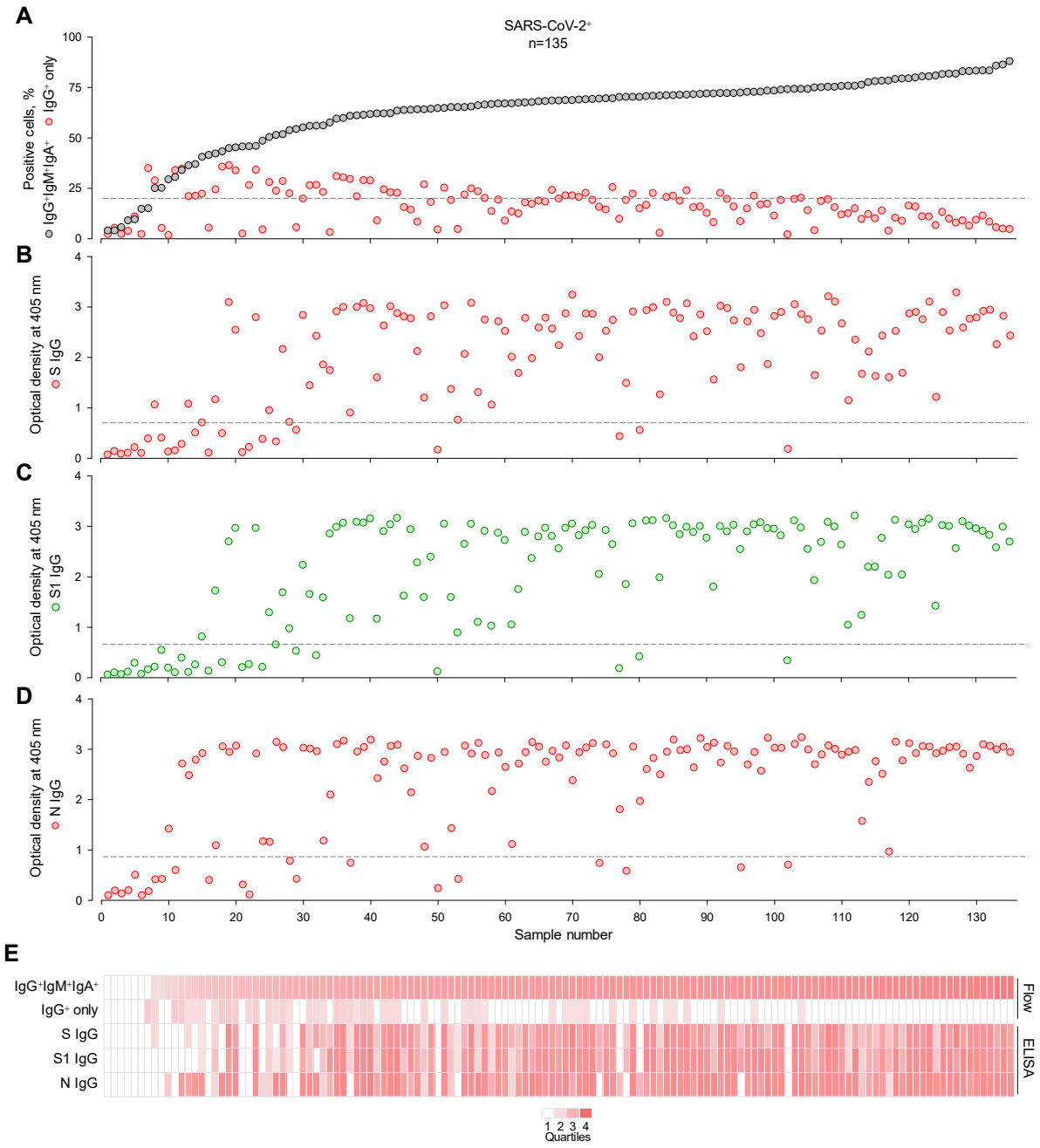

Fig. S5. Comparison of antibody detection methods in an extended cohort of COVID-19 patients.

Samples from a total of 135 confirmed COVID-19 patients were tested (Table S1). (**A**) Frequency of cells that stained with all three antibody classes ($IgG^+IgM^+IgA^+$) or only with IgG (IgG^+) in each of these samples, ranked by their $IgG^+IgM^+IgA^+$ frequency. (**B** to **D**) Optical densities from ELISAs coated with S (B), S1 or RBD (C) or N (D) of the same samples. Dashed lines in A to D denote the assay sensitivity cut-offs. (**E**) Summary of the results from A to D, represented as a heatmap of the quartile values.

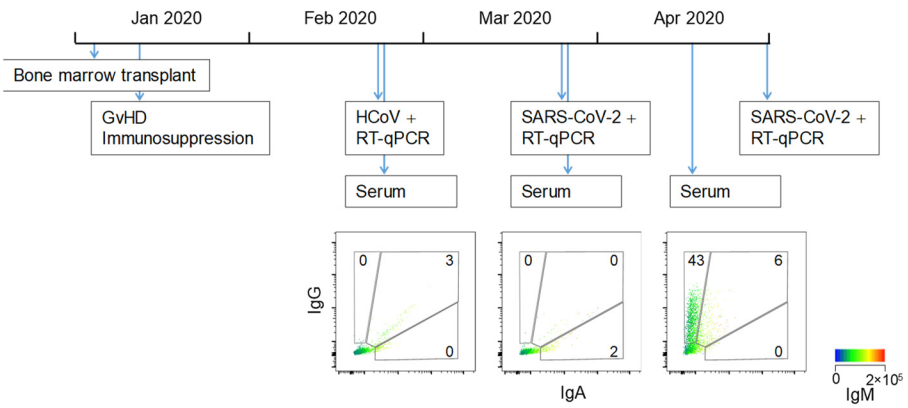

Fig. S6. Sequential HCoV and SARS-CoV-2 infection and clinical observations in an individual case.

A 60-year-old bone-marrow-transplant recipient with graft-versus-host disease (GvHD) and associated immunosuppression tested positive by RT-qPCR for HCoV in February 2020. The patient's sera did not contain SARS-CoV-2 S-binding antibodies at that time. The patient later acquired likely nosocomial SARS-CoV-2 infection with first RT-qPCR confirmation in March 2020. The patient's sera remained negative for SARS-CoV-2 S-binding antibodies at the second sampling time-point, but exhibited IgG reactivity to SARS-CoV-2 S in the absence of IgM or IgA reactivity ($IgG^+IgM^-IgA^-$ profile) 3 weeks later (April 2020). The patient experienced mild COVID-19 symptoms that did not require hospitalization, but remained positive for SARS-CoV-2 infection, with RT-qPCR confirmation in late April 2020. None of the serial serum samples had significant neutralizing activity against SARS-CoV-2 pseudotypes. The $IgG^+IgM^-IgA^-$ flow cytometry profile was observed in only one other patient, 16 days post mild COVID-19 symptoms. This was an 81-year-old patient, who also exhibited IgG reactivity to SARS-CoV-2 S, but not to S1 on ELISA (fig. S4), which would be more characteristic of pre-existing antibody memory to HCoVs, than a de novo response to SARS-CoV-2.

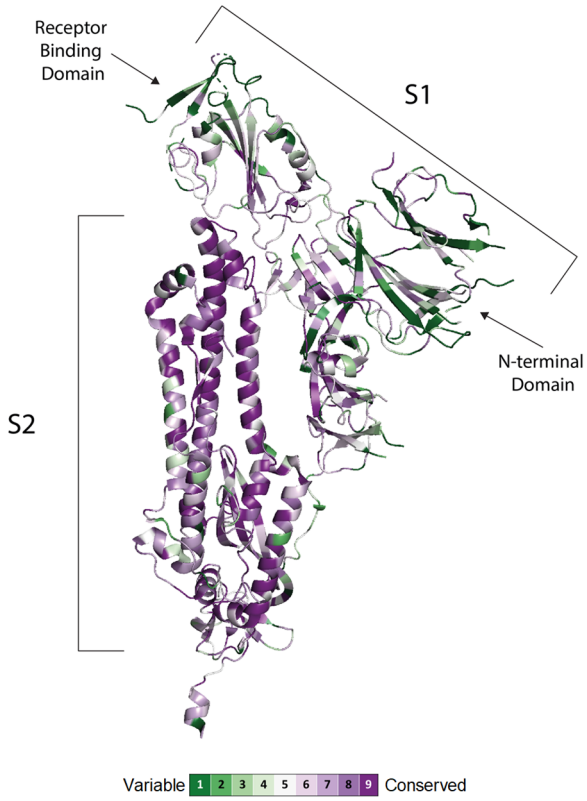

Fig. S7. Conservation of SARS-CoV-2 S subunits.

Structure of the SARS-CoV-2 S protomer with each amino acid residue colored according to conservation among 24 animal and human CoVs. The alignment and the figure were generated using the ConSurf algorithm (https://consurf.tau.ac.il) using a single chain of the SARS-CoV-2 spike protein in the closed state (PDB ID 6VXX) as a reference.

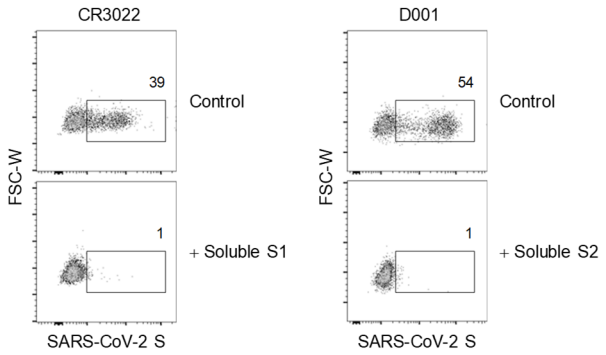

Fig. S8. Competition of antibody binding by recombinant soluble S1 and S2.

HEK293T cells transfected to express SARS-CoV-2 S were stained with the S1-specific CR3022 and S2 specific D001 antibodies in the absence (Control) or in the presence of soluble S1 or S2, respectively. One of two experiments is shown.

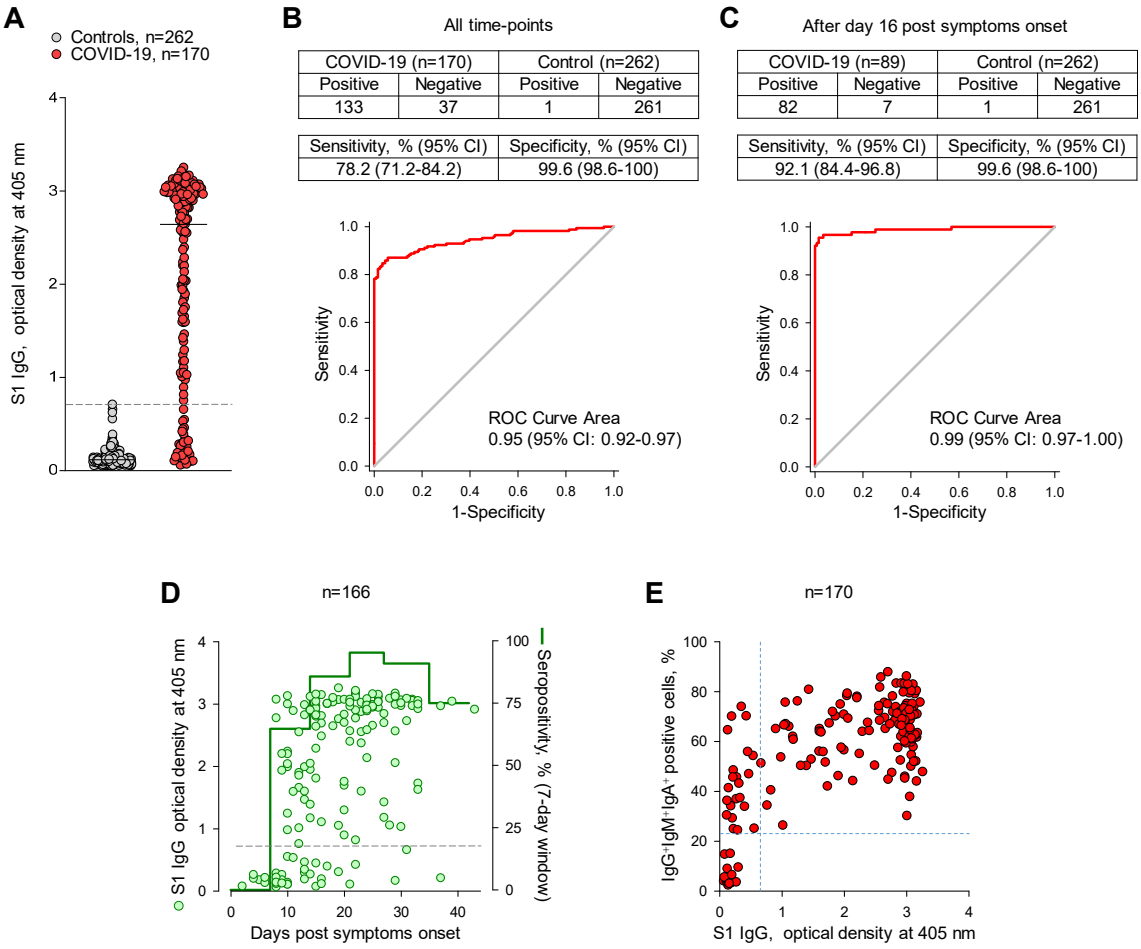

Fig. S9. Performance of the S1 ELISA assay for SARS-CoV-2-reactive antibody detection.

(**A**) Optical densities (ODs) from S1-coated ELISAs on sera from 170 confirmed COVID-19 cases and 262 controls. The dashed line represents the calculate cut-off for positivity. (**B** and **C**) Sensitivity and specificity for the assay calculated for all the sample collected at any time-point post symptom onset (B) or only for samples collected 16 days after the onset of COVID-19 symptoms (C). The receiver operating characteristics (ROC) curve areas and 95% confidence intervals (CI) are also shown for each group. (**D**) Kinetics of seroconversion in COVID-19 patients determined by the S1-coated ELISA. ODs are plotted over time of sample collection since symptom onset. Seropositivity was calculated for each consecutive week since symptom onset. Only COVID-19 patients with known date of symptom onset are included. (**E**) Correlation of seropositivity determined by the S1-coated ELISA and the flow cytometry-based assay. Each symbol represents an individual COVID-19 patient sample.

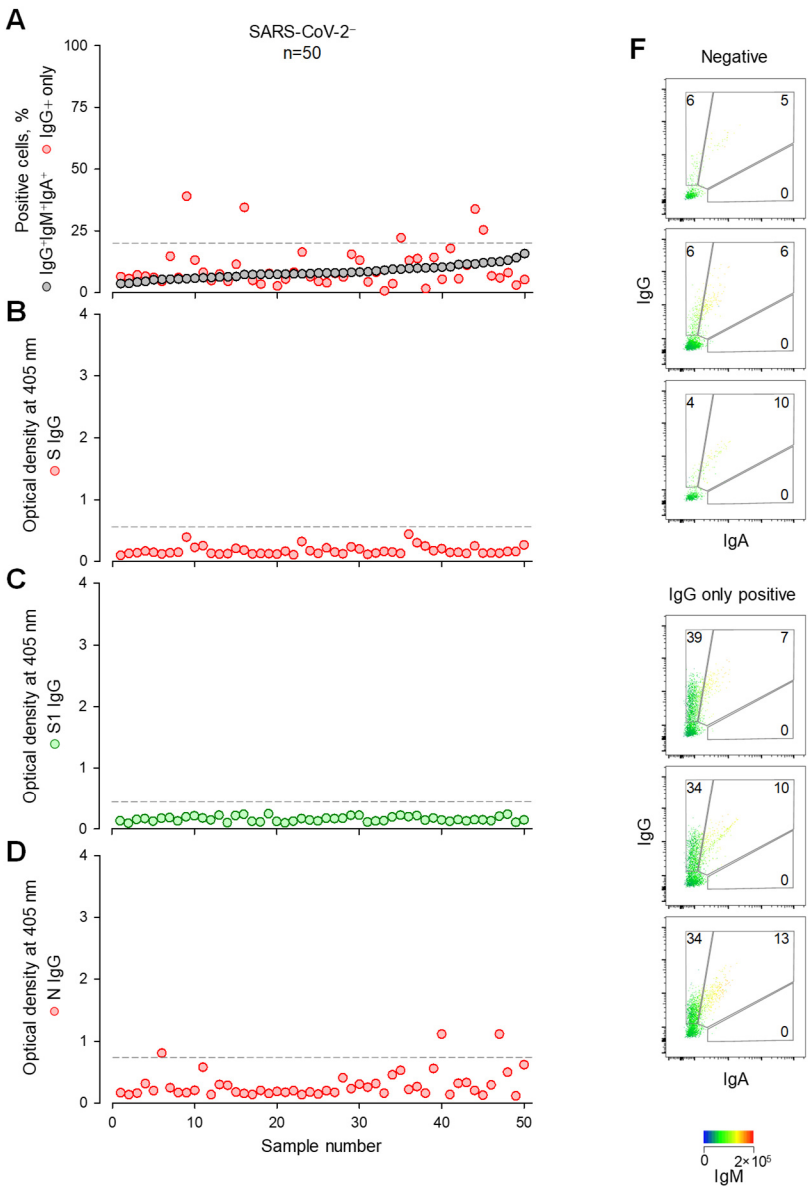

Fig. S10. SARS-CoV-2-reactive antibody detection in an additional control cohort.

Samples from a total of 50 SARS-CoV-2-uninfected individuals collected in 2018 were tested. All 50 were pregnant healthy women visiting antenatal clinics (Table S1). (**A**) Frequency of cells that stained with all three antibody classes ($IgG^+IgM^+IgA^+$) or only with IgG (IgG^+) in each of these samples, ranked by their $IgG^+IgM^+IgA^+$ frequency. (**B** to **D**) Optical densities from ELISAs coated with S (B), S1 or RBD (C) or N (D) of the same samples. Dashed lines in A to D denote the assay sensitivity cut-offs. (**E**) Summary of the results from A to D, represented as a heatmap of the quartile values. (**F**) Representative samples that are negative for all Ig classes (Negative) or positive for IgG alone (IgG only positive).

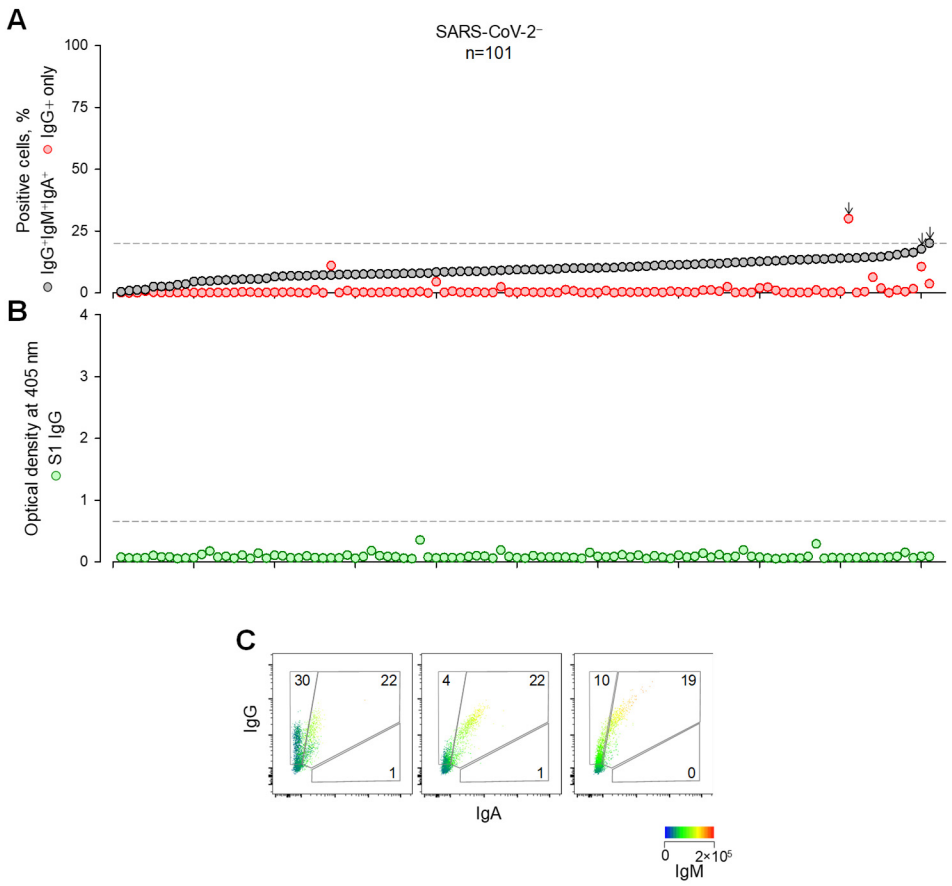

Fig. S11. SARS-CoV-2-reactive antibody detection in an additional control cohort.

Samples from a total of 101 SARS-CoV-2-uninfected individuals collected in 2019 were tested. These included patients with unrelated viral or bacterial infections (Table S1). (**A**) Frequency of cells that stained with all three antibody classes ($IgG^+IgM^+IgA^+$) or only with IgG (IgG^+) in each of these samples, ranked by their $IgG^+IgM^+IgA^+$ frequency. Arrows indicate the three samples with SARS-CoV-2-cross-reactive antibodies. (**B**) Optical densities from S1-coated ELISA of the same samples. Dashed lines in A and B denote the assay sensitivity cut-offs. (**C**) Flow cytometry profiles of the three samples that were positive for SARS-CoV-2-cross-reactive antibodies.

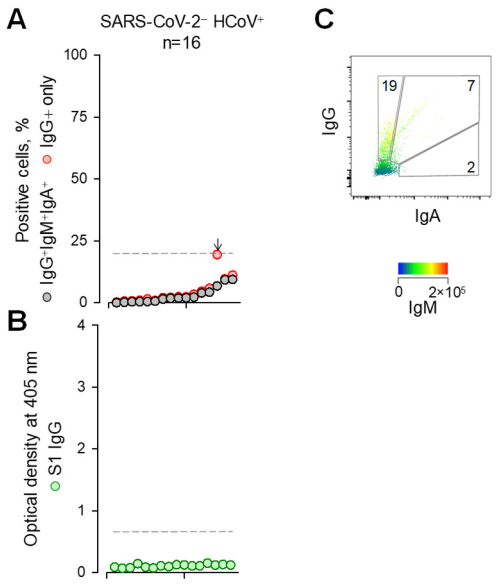

Fig. S12. SARS-CoV-2-reactive antibody detection in an additional control cohort.

A total of 16 samples from 13 individuals with recent HCoV infection (Table S1) were tested. One hematology patient, persistently infected with NL63 was sampled four separate times and all other donors were sampled once. (**A**) Frequency of cells that stained with all three antibody classes ($IgG^+IgM^+IgA^+$) or only with IgG (IgG^+) in each of these samples, ranked by their $IgG^+IgM^+IgA^+$ frequency. The arrow indicate sample with SARS-CoV-2-cross-reactive antibodies. (**B**) Optical densities from S1-coated ELISA of the same samples. Dashed lines in A and B denote the assay sensitivity cut-offs. (**C**) Flow cytometry profile of the sample with SARS-CoV-2-cross-reactive antibodies collected in Jan 2019 from a 66-year-old donor infected with OC43 18 days prior to sampling.

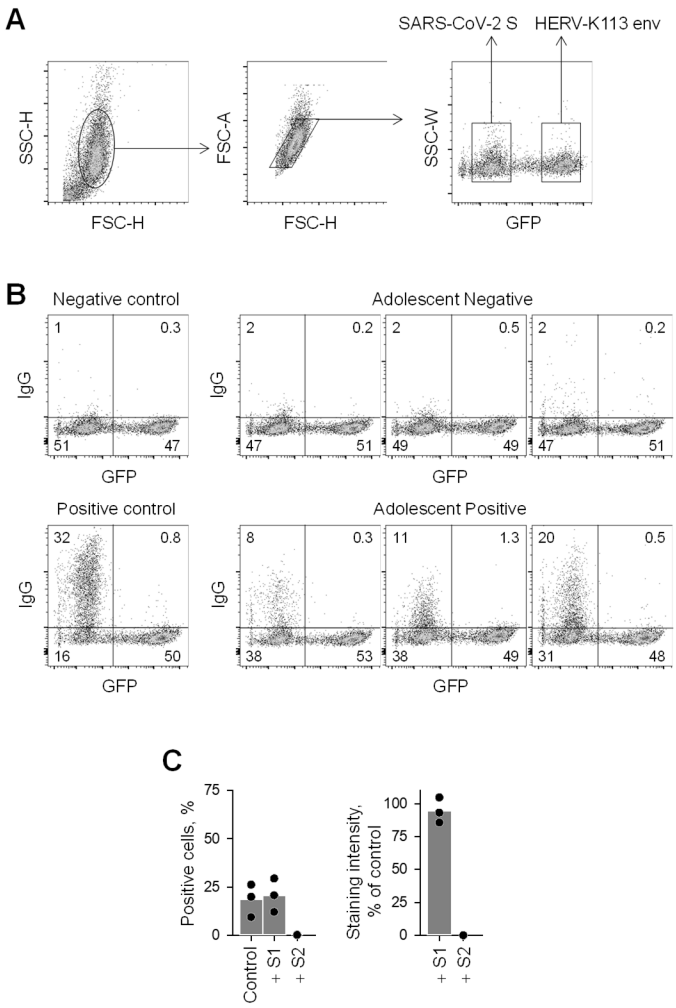

Fig. S13. Specificity controls for SARS-CoV-2 S-reactive antibodies in SARS-CoV-2-uninfected adolescents.

(**A**) Gating strategy for identification of HEK293T cells transfected to express SARS-CoV-2 S (transfection efficiency ~67%) mixed at equal ratios with HEK293T cells homogeneously expressing HERV-K113 envelope glycoprotein (env) and GFP. (**B**) Flow cytometry profiles of a patient without SARS-CoV-2 S-reactive antibodies (Negative control), a seroconverted COVID-19 patient (Positive control) and six samples from SARS-CoV-2-uninfected adolescents, of which three were negative (Adolescent Negative) and three were positive (Adolescent Positive) for SARS-CoV-2-cross-reactive antibodies. No staining of HERV-K113 env-expressing HEK293T cells in the same samples was observed. (**C**) Quantitation of the inhibitory effect of soluble S1 or S2 on binding of three SARS-CoV-2-uninfected adolescent donor sera to SARS-CoV-2 S-expressing HEK293T cells. Mean frequency of positive cells (left) and mean staining intensity (MFI of sample as a percentage of negative control MFI) (right). Each dot represents an individual sample from one of two similar experiments.

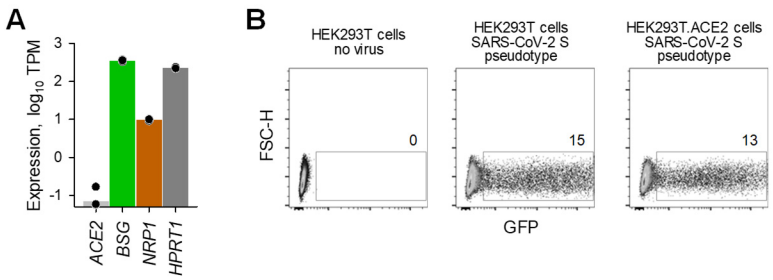

Fig. S14. Entry of SARS-CoV-2 S pseudotypes in HEK293T cells.

(**A**) Expression, plotted as transcripts per million (TPM), of *ACE2*, *BSG*, (encoding CD147), *NRP1* (encoding neuropilin 1) and *HPRT1* in public RNA-sequencing data (GSE85164) from HEK293T cells. (**B**) Transduction efficiency of parental HEK293T cells and HEK293T cells overexpressing ACE2 (HEK293T.ACE2) with GFP-encoding SARS-CoV-2 S pseudotyped lentiviral particles.

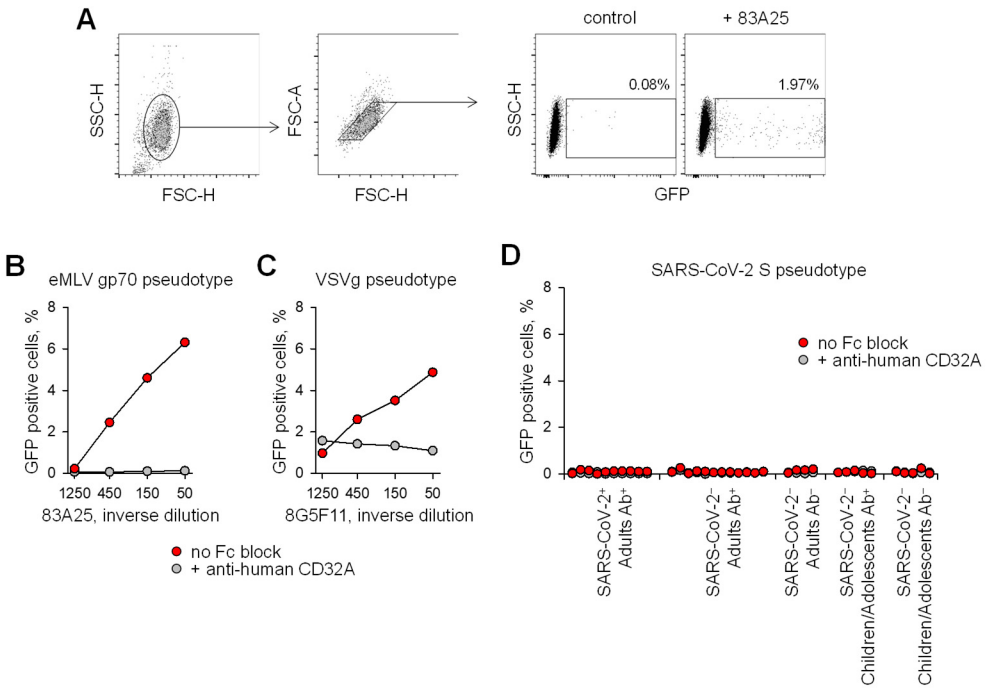

Fig. S15. Assay for antibody-mediated enhancement (ADE) by SARS-CoV-2 S-reactive antibodies.

(**A**) Gating strategy for K-562 cells transduced by an ecotropic MLV envelope glycoprotein (eMLV gp70)-pseudotyped vector expressing GFP. Human cells lack the receptor for eMLV gp70 and are therefore resistant to transduction with such pseudotypes (Control). Addition of the MLV envelope glycoprotein-specific 83A25 monoclonal antibody renders K-562 cells permissive to transduction through ADE and serves as one positive control. (**B** and **C**) Quantitation of K-562 cell transduction by eMLV gp70 or VSVg pseudotypes enhanced by 83A25 and 8G5F11 antibodies, respectively, in the absence or presence of the Fc receptor-blocking anti-CD32A antibody. (**D**) Quantitation of K-562 cell transduction enhancement by sera from the indicated patient groups, in the absence or presence of the Fc receptor-blocking anti-CD32A antibody. Each symbol represents an individual patient. One representative of two experiments is shown.

A

Amino acid similarity with SARS-CoV-2 S

	consensus positions, %	identity positions, %
OC43 S	37.9	26.4
HKU1 S	37.0	25.3
229E S	33.4	21.6
NL63 S	32.8	20.5

B

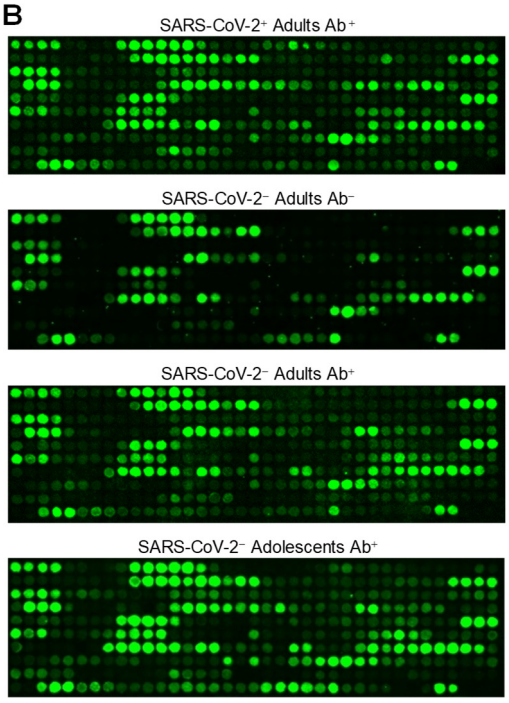

Fig. S16. Mapping of cross-reactive epitopes in SARS-CoV-2 S using peptide arrays.
(**A**) Amino acid sequence similarity and identity between SARS-CoV-2 S and the S proteins of each of the four types of HCoV. (**B**) Scanned images of peptide arrays spanning the last 743 amino acids of SARS-CoV-2 S detected with primary sera from seroconverted COVID-19 patients (SARS-CoV-2$^+$ Adults Ab$^+$), adult SARS-CoV-2-uninfected donors without cross-reactive antibodies detectable by flow cytometry (SARS-CoV-2$^-$ Adults Ab$^-$), and adult and adolescent SARS-CoV-2-uninfected donors that had cross-reactive antibodies detectable by flow cytometry (SARS-CoV-2$^-$ Adults Ab$^+$ and SARS-CoV-2$^-$ Adolescents Ab$^+$, respectively). The signal of the secondary antibody label (IRDye 800CW) is shown in green. The top left position in each array is the first peptide in the sequence ($S_{531\text{-}542}$). The 12-mer peptides were arranged from left-to-right and top-to-bottom with an overlap of 10 amino acids, creating 367 spots.

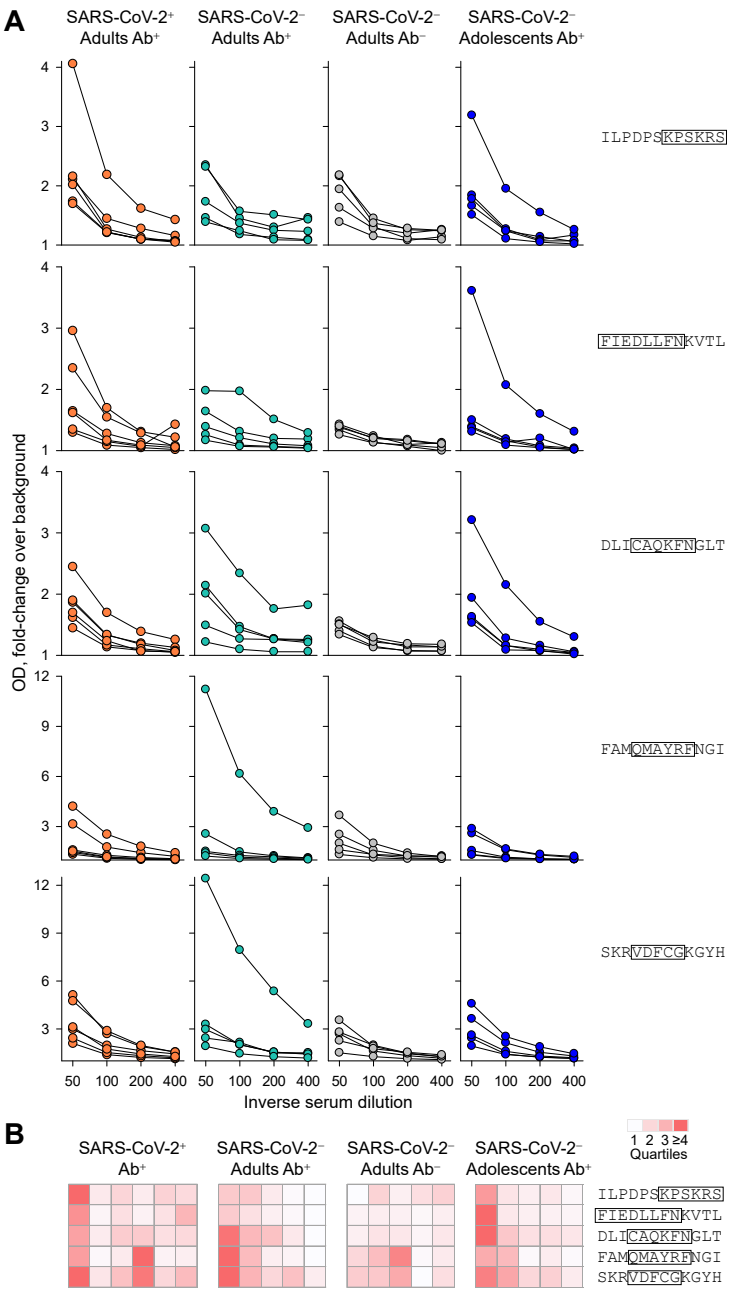

Fig. S17. Reactivity against shared peptide epitopes determined by ELISA.

Sera from seroconverted COVID-19 patients (SARS-CoV-2$^+$ Adults Ab$^+$, n=6), flow cytometry-seronegative SARS-CoV-2-uninfected adults (SARS-CoV-2$^-$ Adults Ab$^-$, n=5), and adult and adolescent SARS-CoV-2-uninfected donors with flow cytometry-detectable cross-reactive antibodies (SARS-CoV-2$^-$ Adults Ab$^+$, n=5 and SARS-CoV-2$^-$ Adolescents Ab$^+$, n=5, respectively), were used in ELISAs coated with the indicated peptides. (**A**) Results are shown as fold-change between sample ODs and ODs of negative control wells. Each line represents an individual sample over the indicated serial dilutions. (**B**) Summary of reactivity of individual sera from the four indicated groups. Each column is an individual sample at 1:50 dilution, represented as a heatmap.

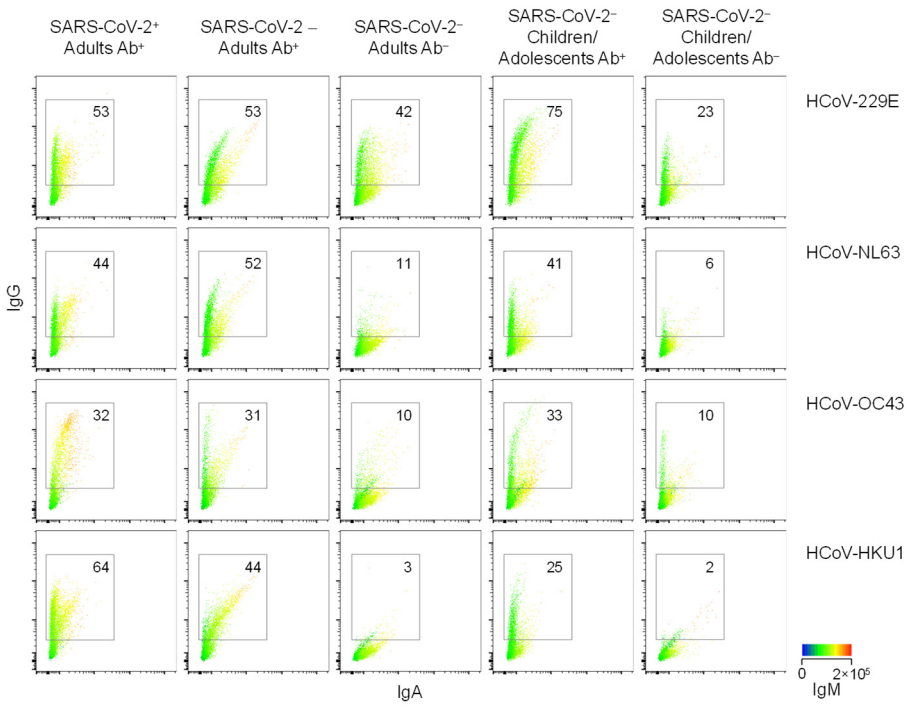

Fig. S18. Reactivity against the S glycoproteins of HCoVs determined by flow cytometry.

Flow cytometry profiles of HEK293T cells transfected to express the S glycoproteins of each of the four HCoVs and stained with the indicated sera (at 1:50 dilution). The same representative sample for each group is shown for all HCoVs for consistency. The groups include seroconverted adult COVID-19 patients (SARS-CoV-2^{+} Adults Ab^{+}); SARS-CoV-2-uninfected adults or children/adolescents with (SARS-CoV-2$^{–}$ Adults Ab^{+} and SARS-CoV-2$^{–}$ Children/Adolescents Ab^{+}, respectively) or without (SARS-CoV-2$^{–}$ Adults Ab$^{–}$ and SARS-CoV-2$^{–}$ Children/Adolescents Ab$^{–}$, respectively) flow cytometry-detectable antibodies cross-reactive with SARS-CoV-2 S. Levels of IgA and IgG are indicates in the *x* and *y* axes, respectively, and levels of IgM are indicated by a heatmap. Numbers within the plots denote the percentage of cells stained with IgG antibodies, irrespective of co-staining with IgM or IgA. Those stained with IgM or IgA are not shown here, but are summarized in Fig. 4D.

Table S1. Details of patient and healthy donor samples used in this study.

Number of donors	Median age (range)	Date of blood collection	Median number of days (range) since	
			symptom onset	RT-qPCR confirmation
A. Initial cohort of COVID-19 patients				
35	64 (24-90)	3/2020-4/2020	14 (5-29)	8 (−3-17)
Patients at UCLH. Age was available for 31 patients.				
B. Extended cohort of COVID-19 patients				
135	64 (36-90)	4/2020	20 (2-43)	13 (−1-33)
Patients at UCLH. Age was available for 80 patients.				
C. SARS-CoV-2-uninfected patients without recent HCoV infection (SARS-CoV-2$^-$ HCoV$^-$)				
31	n/a	8/2019-9/2019	n/a	n/a
Haematology patients at UCLH testing negative for HCoV infection.				
D. SARS-CoV-2-uninfected patients with recent HCoV infection (SARS-CoV-2$^-$ HCoV$^+$)				
34	n/a	12/2019-3/2020	n/a	18 (−5-119)
Haematology patients at UCLH testing positive for HCoV infection.				
E. SARS-CoV-2-uninfected patients of unknown recent HCoV status (SARS-CoV-2$^-$)				
30	n/a	8/2019-9/2019	n/a	n/a
Patients at UCLH, not tested for HCoV infection.				
F. SARS-CoV-2-uninfected pregnant women				
50	32 (17-52)	5/2018	n/a	n/a
Healthy visitors of antenatal clinics at UCLH.				
G. SARS-CoV-2-uninfected patients with unrelated infections				
101	31 (18-65)	5/2019	n/a	n/a
Patients tested at UCLH. They include patients testing positive for antibodies to Influenza HA (2), HBV S (13), HBV C (4), HAV (1), EBV (1), VZV (1), *Borrelia* sp. (Lyme disease) (1), and *Treponema* sp. (syphilis) (1).				

continued on the next page

Number of donors	Median age (range)	Date of blood collection	Median number of days (range) since	
			symptom onset	RT-qPCR confirmation
H. SARS-CoV-2-uninfected patients with recent HCoV infection of known type				
13	52 (21-75)	1/2019-4/2020	n/a	18 (12-55)
Patients at University Hospital of Wales. A total of 16 samples were taken from these 13 patients. One hematology patient, persistently infected with NL63 was sampled four separate times and all other donors were sampled once. They included patients infected with OC43 (5), NL63 (3), 229E (2), and HKU1 (3). The only sample with cross-reactive antibodies was collected in Jan 2019.				
I. SARS-CoV-2-uninfected healthy children and adolescents				
48	14 (1-16)	4/2011-12/2018	n/a	n/a
Samples were from healthy volunteers at the UCL Centre for Adolescent Rheumatology, Great Ormond Street (GOSH) Institute for Child Health (ICH) and Adolescent Centre Biobank.				
J. SARS-CoV-2-uninfected healthy young adults				
43	21 (17-25)	2/2013-2/2020	n/a	n/a
Samples were from healthy volunteers at the UCL Centre for Adolescent Rheumatology, Great Ormond Street (GOSH) Institute for Child Health (ICH) and Adolescent Centre Biobank.				

Table S2. Cross-reactive epitopes identified in SARS-CoV-2 S.

Epitope position	Core epitope sequence	Position in the trimeric S structure (PDB ID: 6ZGE)	Comments
$S_{810-816}$	SKPSKRS	Surface; fusion peptide.	Computationally predicted in SARS-CoV-2 (*36*).
$S_{817-824}$	FIEDLLFN	Surface; fusion peptide	Identified as cross-reactive in HCoV-OC43 and HCoV-229E (*11*).
$S_{851-856}$	CAQKFN	Recently solved surface loop (*37*).	
$S_{901-906}$	QMAYRF	Surface.	Experimentally defined in SARS-CoV (*36*).
$S_{997-1002}$	ITGRLQ	Not exposed in pre-fusion S conformation.	Accessible in alternative conformations (*38-40*).
$S_{1040-1044}$	VDFCG	Surface.	
$S_{1205-1212}$	KYEQYIKW	Membrane-proximal region.	Not part of current structures.

References

1. R. W. Aldridge, D. Lewer, S. Beale, A. M. Johnson, M. Zambon, A. C. Hayward, E. B. Fragaszy, Seasonality and immunity to laboratory-confirmed seasonal coronaviruses (HCoV-NL63, HCoV-OC43, and HCoV-229E): Results from the Flu Watch cohort study. *Wellcome Open Res.* **5**, 52 (2020). doi:10.12688/wellcomeopenres.15812.1

2. K. A. Callow, H. F. Parry, M. Sergeant, D. A. Tyrrell, The time course of the immune response to experimental coronavirus infection of man. *Epidemiol. Infect.* **105**, 435–446 (1990). doi:10.1017/S0950268800048019 Medline

3. E. G. Severance, I. Bossis, F. B. Dickerson, C. R. Stallings, A. E. Origoni, A. Sullens, R. H. Yolken, R. P. Viscidi, Development of a nucleocapsid-based human coronavirus immunoassay and estimates of individuals exposed to coronavirus in a U.S. metropolitan population. *Clin. Vaccine Immunol.* **15**, 1805–1810 (2008). doi:10.1128/CVI.00124-08 Medline

4. R. Dijkman, M. F. Jebbink, N. B. El Idrissi, K. Pyrc, M. A. Müller, T. W. Kuijpers, H. L. Zaaijer, L. van der Hoek, Human coronavirus NL63 and 229E seroconversion in children. *J. Clin. Microbiol.* **46**, 2368–2373 (2008). doi:10.1128/JCM.00533-08 Medline

5. A. T. Huang, B. Garcia-Carreras, M. D. T. Hitchings, B. Yang, L. C. Katzelnick, S. M. Rattigan, B. A. Borgert, C. A. Moreno, B. D. Solomon, L. Trimmer-Smith, V. Etienne, I. Rodriguez-Barraquer, J. Lessler, H. Salje, D. S. Burke, A. Wesolowski, D. A. T. Cummings, A systematic review of antibody mediated immunity to coronaviruses: Kinetics, correlates of protection, and association with severity. *Nat. Commun.* **11**, 4704 (2020). doi:10.1038/s41467-020-18450-4 Medline

6. N. Friedman, H. Alter, M. Hindiyeh, E. Mendelson, Y. Shemer Avni, M. Mandelboim, Human coronavirus infections in Israel: Epidemiology, clinical symptoms and summer seasonality of HCoV-HKU1. *Viruses* **10**, 515 (2018). doi:10.3390/v10100515 Medline

7. S. Nickbakhsh *et al*., Epidemiology of seasonal coronaviruses: Establishing the context for COVID-19 emergence. *J. Infect. Dis.* (2020).

8. A. S. Monto, P. M. DeJonge, A. P. Callear, L. A. Bazzi, S. B. Capriola, R. E. Malosh, E. T. Martin, J. G. Petrie, Coronavirus occurrence and transmission over 8 years in the HIVE cohort of households in Michigan. *J. Infect. Dis.* **222**, 9–16 (2020). doi:10.1093/infdis/jiaa161 Medline

9. X. Chi, R. Yan, J. Zhang, G. Zhang, Y. Zhang, M. Hao, Z. Zhang, P. Fan, Y. Dong, Y. Yang, Z. Chen, Y. Guo, J. Zhang, Y. Li, X. Song, Y. Chen, L. Xia, L. Fu, L. Hou, J. Xu, C. Yu, J. Li, Q. Zhou, W. Chen, A neutralizing human antibody binds to the N-terminal domain of the Spike protein of SARS-CoV-2. *Science* **369**, 650–655 (2020). doi:10.1126/science.abc6952 Medline

10. G. Song, W. He, S. Callaghan, F. Anzanello, D. Huang, J. Ricketts, J. L. Torres, N. Beutler, L. Peng, S. Vargas, J. Cassell, M. Parren, L. Yang, C. Ignacio, D. M. Smith, J. E. Voss, D. Nemazee, A. B. Ward, T. Rogers, D. R. Burton, R. Andrabi, Cross-reactive serum and memory B cell responses to spike protein in SARS-CoV-2 and endemic coronavirus infection. bioRxiv 308965 [Preprint]. 23 September 2020; https://doi.org/10.1101/2020.09.22.308965.

11. E. Shrock, E. Fujimura, T. Kula, R. T. Timms, I.-H. Lee, Y. Leng, M. L. Robinson, B. M. Sie, M. Z. Li, Y. Chen, J. Logue, A. Zuiani, D. McCulloch, F. J. N. Lelis, S. Henson, D. R. Monaco, M. Travers, S. Habibi, W. A. Clarke, P. Caturegli, O. Laeyendecker, A. Piechocka-Trocha, J. Li, A. Khatri, H. Y. Chu, A.-C. Villani, K. Kays, M. B. Goldberg, N. Hacohen, M. R. Filbin, X. G. Yu, B. D. Walker, D. R. Wesemann, H. B. Larman, J. A. Lederer, S. J. Elledge; MGH COVID-19 Collection & Processing Team, Viral epitope profiling of COVID-19 patients reveals cross-reactivity and correlates of severity. *Science* eabd4250 (2020). doi:10.1126/science.abd4250 Medline

12. A. Grifoni, D. Weiskopf, S. I. Ramirez, J. Mateus, J. M. Dan, C. R. Moderbacher, S. A. Rawlings, A. Sutherland, L. Premkumar, R. S. Jadi, D. Marrama, A. M. de Silva, A. Frazier, A. F. Carlin, J. A. Greenbaum, B. Peters, F. Krammer, D. M. Smith, S. Crotty, A. Sette, Targets of T cell responses to SARS-CoV-2 coronavirus in humans with COVID-19 disease and unexposed individuals. *Cell* **181**, 1489–1501.e15 (2020). doi:10.1016/j.cell.2020.05.015 Medline

13. J. Braun, L. Loyal, M. Frentsch, D. Wendisch, P. Georg, F. Kurth, S. Hippenstiel, M. Dingeldey, B. Kruse, F. Fauchere, E. Baysal, M. Mangold, L. Henze, R. Lauster, M. A. Mall, K. Beyer, J. Röhmel, S. Voigt, J. Schmitz, S. Miltenyi, I. Demuth, M. A. Müller, A. Hocke, M. Witzenrath, N. Suttorp, F. Kern, U. Reimer, H. Wenschuh, C. Drosten, V. M. Corman, C. Giesecke-Thiel, L. E. Sander, A. Thiel, SARS-CoV-2-reactive T cells in healthy donors and patients with COVID-19. *Nature* (2020). doi:10.1038/s41586-020-2598-9 Medline

14. N. Le Bert, A. T. Tan, K. Kunasegaran, C. Y. L. Tham, M. Hafezi, A. Chia, M. H. Y. Chng, M. Lin, N. Tan, M. Linster, W. N. Chia, M. I.-C. Chen, L.-F. Wang, E. E. Ooi, S. Kalimuddin, P. A. Tambyah, J. G.-H. Low, Y.-J. Tan, A. Bertoletti, SARS-CoV-2-specific T cell immunity in cases of COVID-19 and SARS, and uninfected controls. *Nature* **584**, 457–462 (2020). doi:10.1038/s41586-020-2550-z Medline

15. P. Nguyen-Contant, A. K. Embong, P. Kanagaiah, F. A. Chaves, H. Yang, A. R. Branche, D. J. Topham, M. Y. Sangster, S protein-reactive IgG and memory B cell production after human SARS-CoV-2 infection includes broad reactivity to the S2 subunit. *mBio* **11**, e01991–e01920 (2020). doi:10.1128/mBio.01991-20 Medline

16. P. K. Kiyuka, C. N. Agoti, P. K. Munywoki, R. Njeru, A. Bett, J. R. Otieno, G. P. Otieno, E. Kamau, T. G. Clark, L. van der Hoek, P. Kellam, D. J. Nokes, M. Cotten, Human coronavirus NL63 molecular epidemiology and evolutionary patterns in rural coastal Kenya. *J. Infect. Dis.* **217**, 1728–1739 (2018). doi:10.1093/infdis/jiy098 Medline

17. R. Castagnoli, M. Votto, A. Licari, I. Brambilla, R. Bruno, S. Perlini, F. Rovida, F. Baldanti, G. L. Marseglia, Severe acute respiratory syndrome coronavirus 2 (SARS-CoV-2) infection in children and adolescents: A systematic review. *JAMA Pediatr.* **174**, 882–889 (2020). doi:10.1001/jamapediatrics.2020.1467 Medline

18. P. R. Grant, M. A. Turner, G. Y. Shin, E. Nastouli, L. J. Levett, Extraction-free COVID-19 (SARS-CoV-2) diagnosis by RT-PCR to increase capacity for national testing programmes during a pandemic. bioRxiv 028316 [Preprint]. 9 April 2020; https://doi.org/10.1101/2020.04.06.028316.

19. K. Hanke, P. Kramer, S. Seeher, N. Beimforde, R. Kurth, N. Bannert, Reconstitution of the ancestral glycoprotein of human endogenous retrovirus k and modulation of its functional activity by truncation of the cytoplasmic domain. *J. Virol.* **83**, 12790–12800 (2009). doi:10.1128/JVI.01368-09 Medline

20. J. ter Meulen, E. N. van den Brink, L. L. M. Poon, W. E. Marissen, C. S. W. Leung, F. Cox, C. Y. Cheung, A. Q. Bakker, J. A. Bogaards, E. van Deventer, W. Preiser, H. W. Doerr, V. T. Chow, J. de Kruif, J. S. M. Peiris, J. Goudsmit, Human monoclonal antibody combination against SARS coronavirus: Synergy and coverage of escape mutants. *PLOS Med.* **3**, e237 (2006). doi:10.1371/journal.pmed.0030237 Medline

21. M. G. Joyce, R. S. Sankhala, W.-H. Chen, M. Choe, H. Bai, A. Hajduczki, L. Yan, S. L. Sterling, C. E. Peterson, E. C. Green, C. Smith, N. de Val, M. Amare, P. Scott, E. D. Laing, C. C. Broder, M. Rolland, N. L. Michael, K. Modjarrad, A cryptic site of vulnerability on the receptor binding domain of the SARS-CoV-2 spike glycoprotein. bioRxiv 992883 [Preprint]. 17 March 2020; https://doi.org/10.1101/2020.03.15.992883.

22. V. E. Pye, A. Rosa, C. Bertelli, W. B. Struwe, S. L. Maslen, R. Corey, I. Liko, M. Hassall, G. Mattiuzzo, A. Ballandras-Colas, A. Nans, Y. Takeuchi, P. J. Stansfeld, J. M. Skehel, C. V. Robinson, M. Pizzato, P. Cherepanov, A bipartite structural organization defines the SERINC family of HIV-1 restriction factors. *Nat. Struct. Mol. Biol.* **27**, 78–83 (2020). doi:10.1038/s41594-019-0357-0 Medline

23. J. Pallesen, N. Wang, K. S. Corbett, D. Wrapp, R. N. Kirchdoerfer, H. L. Turner, C. A. Cottrell, M. M. Becker, L. Wang, W. Shi, W.-P. Kong, E. L. Andres, A. N. Kettenbach, M. R. Denison, J. D. Chappell, B. S. Graham, A. B. Ward, J. S. McLellan, Immunogenicity and structures of a rationally designed prefusion MERS-CoV spike antigen. *Proc. Natl. Acad. Sci. U.S.A.* **114**, E7348–E7357 (2017). doi:10.1073/pnas.1707304114 Medline

24. D. Wrapp, N. Wang, K. S. Corbett, J. A. Goldsmith, C.-L. Hsieh, O. Abiona, B. S. Graham, J. S. McLellan, Cryo-EM structure of the 2019-nCoV spike in the prefusion conformation. *Science* **367**, 1260–1263 (2020). doi:10.1126/science.abb2507 Medline

25. Y. Lin, Y. Gu, S. A. Wharton, L. Whittaker, V. Gregory, X. Li, S. Metin, N. Cattle, R. S. Daniels, A. J. Hay, J. W. McCauley, Optimisation of a micro-neutralisation assay and its application in antigenic characterisation of influenza viruses. *Influenza Other Respir. Viruses* **9**, 331–340 (2015). doi:10.1111/irv.12333 Medline

26. L. H. Evans, R. P. Morrison, F. G. Malik, J. Portis, W. J. Britt, A neutralizable epitope common to the envelope glycoproteins of ecotropic, polytropic, xenotropic, and amphotropic murine leukemia viruses. *J. Virol.* **64**, 6176–6183 (1990). doi:10.1128/JVI.64.12.6176-6183.1990 Medline

27. M. Hoffmann, H. Kleine-Weber, S. Schroeder, N. Krüger, T. Herrler, S. Erichsen, T. S. Schiergens, G. Herrler, N.-H. Wu, A. Nitsche, M. A. Müller, C. Drosten, S. Pöhlmann, SARS-CoV-2 cell entry depends on ACE2 and TMPRSS2 and is blocked by a clinically proven protease inhibitor. *Cell* **181**, 271–280.e8 (2020). doi:10.1016/j.cell.2020.02.052 Medline

28. X. Ou, Y. Liu, X. Lei, P. Li, D. Mi, L. Ren, L. Guo, R. Guo, T. Chen, J. Hu, Z. Xiang, Z. Mu, X. Chen, J. Chen, K. Hu, Q. Jin, J. Wang, Z. Qian, Characterization of spike glycoprotein of SARS-CoV-2 on virus entry and its immune cross-reactivity with SARS-CoV. *Nat. Commun.* **11**, 1620 (2020). doi:10.1038/s41467-020-15562-9 Medline

29. A. C. Walls, Y. J. Park, M. A. Tortorici, A. Wall, A. T. McGuire, D. Veesler, Structure, Function, and Antigenicity of the SARS-CoV-2 Spike Glycoprotein. *Cell* **181**, 281–292.e6 (2020). doi:10.1016/j.cell.2020.02.058 Medline

30. P. Zhou, X. L. Yang, X. G. Wang, B. Hu, L. Zhang, W. Zhang, H. R. Si, Y. Zhu, B. Li, C. L. Huang, H. D. Chen, J. Chen, Y. Luo, H. Guo, R. D. Jiang, M. Q. Liu, Y. Chen, X. R. Shen, X. Wang, X. S. Zheng, K. Zhao, Q. J. Chen, F. Deng, L. L. Liu, B. Yan, F. X. Zhan, Y. Y. Wang, G. F. Xiao, Z. L. Shi, A pneumonia outbreak associated with a new coronavirus of probable bat origin. *Nature* **579**, 270–273 (2020). doi:10.1038/s41586-020-2012-7 Medline

31. K. Wang, W. Chen, Y.-S. Zhou, J.-Q. Lian, Z. Zhang, P. Du, L. Gong, Y. Zhang, H.-Y. Cui, J.-J. Geng, B. Wang, X.-X. Sun, C.-F. Wang, X. Yang, P. Lin, Y.-Q. Deng, D. Wei, X.-M. Yang, Y.-M. Zhu, K. Zhang, Z.-H. Zheng, J.-L. Miao, T. Guo, Y. Shi, J. Zhang, L. Fu, Q.-Y. Wang, H. Bian, P. Zhu, Z.-N. Chen, SARS-CoV-2 invades host cells via a novel route: CD147-spike protein. bioRxiv 988345 [Preprint]; 14 March 2020; https://doi.org/10.1101/2020.03.14.988345.

32. L. Cantuti-Castelvetri, R. Ojha, L. D. Pedro, M. Djannatian, J. Franz, S. Kuivanen, K. Kallio, T. Kaya, M. Anastasina, T. Smura, L. Levanov, L. Szirovicza, A. Tobi, H. Kallio-Kokko, P. Österlund, M. Joensuu, F. A. Meunier, S. Butcher, M. S. Winkler, B. Mollenhauer, A. Helenius, O. Gokce, T. Teesalu, J. Hepojoki, O. Vapalahti, C. Stadelmann, G. Balistreri, M. Simons, Neuropilin-1 facilitates SARS-CoV-2 cell entry and provides a possible pathway into the central nervous system. bioRxiv 137802 [Preprint]. 15 July 2020; https://doi.org/10.1101/2020.06.07.137802.

33. J. L. Daly, B. Simonetti, C. Antón-Plágaro, M. Kavanagh Williamson, D. K. Shoemark, L. Simón-Gracia, K. Klein, M. Bauer, R. Hollandi, U. F. Greber, P. Horvath, R. B. Sessions, A. Helenius, J. A. Hiscox, T. Teesalu, D. A. Matthews, A. D. Davidson, P. J. Cullen, Y. Yamauch, Neuropilin-1 is a host factor for SARS-CoV-2 infection. bioRxiv 134114 [Preprint]. 5 June 2020; https://doi.org/10.1101/2020.06.05.134114.

34. M. C. Freeman, C. T. Peek, M. M. Becker, E. C. Smith, M. R. Denison, Coronaviruses induce entry-independent, continuous macropinocytosis. *mBio* **5**, e01340–e14 (2014). doi:10.1128/mBio.01340-14 Medline

35. T. C. Nash, T. M. Gallagher, M. J. Buchmeier, MHVR-independent cell-cell spread of mouse hepatitis virus infection requires neutral pH fusion. *Adv. Exp. Med. Biol.* **380**, 351–357 (1995). doi:10.1007/978-1-4615-1899-0_57 Medline

36. A. Grifoni, J. Sidney, Y. Zhang, R. H. Scheuermann, B. Peters, A. Sette, A Sequence Homology and Bioinformatic Approach Can Predict Candidate Targets for Immune Responses to SARS-CoV-2. *Cell Host Microbe* **27**, 671–680.e2 (2020). doi:10.1016/j.chom.2020.03.002 Medline

37. A. G. Wrobel, D. J. Benton, P. Xu, C. Roustan, S. R. Martin, P. B. Rosenthal, J. J. Skehel, S. J. Gamblin, SARS-CoV-2 and bat RaTG13 spike glycoprotein structures inform on virus evolution and furin-cleavage effects. *Nat. Struct. Mol. Biol.* **27**, 763–767 (2020). doi:10.1038/s41594-020-0468-7 Medline

38. Y. Cai, J. Zhang, T. Xiao, H. Peng, S. M. Sterling, R. M. Walsh Jr., S. Rawson, S. Rits-Volloch, B. Chen, Distinct conformational states of SARS-CoV-2 spike protein. *Science* **369**, 1586–1592 (2020). doi:10.1126/science.abd4251 Medline

39. B. Turoňová, M. Sikora, C. Schürmann, W. J. H. Hagen, S. Welsch, F. E. C. Blanc, S. von Bülow, M. Gecht, K. Bagola, C. Hörner, G. van Zandbergen, J. Landry, N. T. D. de Azevedo, S. Mosalaganti, A. Schwarz, R. Covino, M. D. Mühlebach, G. Hummer, J. Krijnse Locker, M. Beck, In situ structural analysis of SARS-CoV-2 spike reveals

flexibility mediated by three hinges. *Science* **370**, 203–208 (2020). doi:10.1126/science.abd5223 Medline

40. S. Klein, M. Cortese, S. L. Winter, M. Wachsmuth-Melm, C. J. Neufeldt, B. Cerikan, M. L. Stanifer, S. Boulant, R. Bartenschlager, P. Chlanda, SARS-CoV-2 structure and replication characterized by in situ cryoelectron tomography. bioRxiv 167064 [Preprint]. 16 August 2020; https://doi.org/10.1101/2020.06.23.167064.

Acknowledgements: We thank L. James and J. Luptak for the SARV CoV2 N expression construct and M. Pizzato for the SARS CoV2 S cDNA. We also thank the entire CRICK COVID-19 Consortium. We are grateful for assistance from the Cell Services and High Throughput Screening facilities at the Francis Crick Institute and UCLH Biochemistry (A. Goyale and C. Wilson) and to Mr Michael Bennet and Mr Simon Caidan for training and support in the high-containment laboratory. **Funding:** This work was supported by a Centre of Excellence Centre for Adolescent Rheumatology Versus Arthritis grant, 21593, as well as support from the Great Ormond Street Childrens Charity, CureJM Foundation and the NIHR Biomedical Research Centres at GOSH and UCLH. This work was supported by the Francis Crick Institute, which receives its core funding from Cancer Research UK, the UK Medical Research Council, and the Wellcome Trust. **Author contributions:** Experimental design, C.C., L.R.W., R.B., C.S., S.G., B.S., J.McC., S.J.G., L.E.McC., P.C., E.N., and G.K. Investigation, K.W.N., N.F., G.H.C., A.Ro., R.H., S.H., R.U., C.E., A.G.W., D.J.B., C.R., W.B., R.T., A.A.-D., P.H., and D.J. Reagents and Samples, J.H., H.R., S.P., C.F.H., K.T., E.S., G.Y.S., M.J.S., P.A.W., C.M., B.R.J., M.G.Ll.W., L.R.M., E.C.R., A.Ra., and H.P. Writing, L.E.McC., P.C., E.N., and G.K., with contributions from C.C., L.R.W., K.W.N., N.F., and G.H.C. Supervision, N.O'R., S.K., A.Ri., C.C., L.R.W., R.B., C.S., S.G., B.S., J.McC., S.J.G., L.E.McC., P.C., E.N., and G.K. **Competing interests:** The authors declare no competing interests. **Data and materials availability:** All data are available in the main text or the supplementary materials.

Supplementary Materials

science.sciencemag.org/cgi/content/full/science.abe1107/DC1

Materials and Methods

Supplementary Text

Figs. S1 to S18

Tables S1 and S2

References (*18–40*)

MDAR Reproducibility Checklist

31 July 2020; accepted 29 October 2020

Published online 6 November 2020

Fig. 1. Flow cytometric detection and specificity of antibodies reactive with SARS-CoV-2 S. (**A**) Detection of IgG, IgA, and IgM in five individuals from each indicated group. IgM levels are indicated by a heatmap. (**B** to **D**) Inhibition of SARS-CoV-2 S binding of sera from SARS-CoV-2-infected (SARS-CoV-2$^+$, n=10) or SARS-CoV-2-uninfected (SARS-CoV-2$^-$ HCoV$^+$, n=6) patients by soluble S1 or S2. Flow cytometry profile of one representative patient per group is shown (B). Mean frequency of positive cells (C). **P*=0.015; ***P*=0.006, one-way analysis of variance (ANOVA) on Ranks. Mean staining intensity (mean fluorescent intensity (MFI) of sample as a percentage of negative control MFI) (D). In C and D, dots represent individual samples from one of three similar experiments.

Fig. 2. Prevalence of SARS-CoV-2 S-cross-reactive antibodies detected by different methods. (**A**) Flow cytometry and ELISA results for each sample in cohorts A and C to E (table S1). (**B**) Flow cytometry and ELISA results for serum samples from SARS-CoV-2-uninfected pregnant women. (**C** to **E**) SARS-CoV-2 S-cross-reactive antibodies in healthy children and adolescents. Representative flow cytometry profiles of seronegative donors (Negative) or COVID-19 patients (Positive) and of SARS-CoV-2-uninfected adolescents with SARS-CoV-2-cross-reactive antibodies (C). Frequency of cells stained with all three antibody classes (IgG$^+$IgM$^+$IgA$^+$) or only with IgG (IgG$^+$), ranked by their IgG$^+$IgM$^+$IgA$^+$ frequency (D). The dashed line denotes the assay sensitivity cut-off. Flow cytometry and ELISA results for each sample (E). (**F**) Prevalence of SARS-CoV-2 S-cross-reactive antibodies in the indicated age groups (line) and frequency of cells that stained only with IgG (dots) in all samples for which the date of birth was known. The heatmaps in A, B, and E represent the quartile values above each assay's technical cut-off.

Fig. 3. Neutralization of SARS-CoV-2 S pseudotypes and authentic SARS-CoV-2 by SARS-CoV-2-infected and -uninfected patient sera. (**A**) Inhibition of transduction efficiency of SARS-CoV-2 S or VSVg pseudotypes by adult COVID-19 patients who seroconverted (SARS-CoV-2$^+$ Adults Ab$^+$) or not (SARS-CoV-2$^+$ Adults Ab$^-$), and SARS-CoV-2-uninfected adult (SARS-CoV-2$^-$ Adults Ab$^+$) or children and adolescent donors (SARS-CoV-2$^-$ Children/Adolescents Ab$^+$) donors with SARS-CoV-2 S-binding antibodies. Each line is an individual serum sample. (**B**) Authentic SARS-CoV-2 neutralization titers of sera from the same donors as in A, as well as SARS-CoV-2-uninfected donors without SARS-CoV-2 S-binding antibodies (Ab$^-$). Dots represent individual samples. **P*=0.037; ***P*=0.014; ns: not significant, one-way ANOVA on Ranks.

Fig. 4. Mapping of cross-reactive epitopes in SARS-CoV-2 S. (**A**) Signal intensity for each overlapping peptide along the length of SARS-CoV-2 S covered in the peptide arrays, using pooled sera with (Ab$^+$) or without (Ab$^-$) flow cytometry-detectable SARS-CoV-2 S-reactive antibodies. Differentially recognized peaks are boxed. (**B**) Alignment of the amino acid sequences of SARS-CoV-2 and HCoV S glycoproteins. Boxes indicate predicted core epitopes. (**C**) Mapping of predicted epitopes targeted on the trimeric SARS-CoV-2 spike. The S1 (blue) and S2 (pink) of one monomer are colored. Epitopes are shown for one monomer; the circled dashed line represent the membrane proximal region not present in the structure. (**D**) (Left), Reactivity with the S glycoproteins of each HCoV of the indicated sera with (Ab$^+$) or without (Ab$^-$) flow cytometry-detectable SARS-CoV-2 S-reactive antibodies, determined by flow cytometry. Each column is an individual sample. Rows depict the staining for each antibody class. (Right), Correlation coefficients between percentages of IgG staining for SARS-CoV-2 S and IgG, IgM, and IgA staining for each HCoV S glycoprotein.